Influence of agricultural organic inputs and their aging on the transport of ferrihydrite nanoparticles: From enhancement to inhibition

Science of the Total Environment

Qian, Xiaoyan; Ma, Jie; Weng, Liping; Chen, Yali; Ren, Zongling et al

https://doi.org/10.1016/j.scitotenv.2020.137440

Science of the Total Environment 719 (2020) 137440

Contents lists available at ScienceDirect

Science of the Total Environment

journal homepage: www.elsevier.com/locate/scitotenv

Influence of agricultural organic inputs and their aging on the transport of ferrihydrite nanoparticles: From enhancement to inhibition

Xiaoyan Qian [a,b,1], Jie Ma [a,b,*,1], Liping Weng [a,b,c], Yali Chen [a,b], Zongling Ren [d], Yongtao Li [b,d]

[a] Key Laboratory for Environmental Factors Control of Agro-Product Quality Safety, Ministry of Agriculture and Rural Affairs, Tianjin 300191, China
[b] Agro-Environmental Protection Institute, Ministry of Agriculture and Rural Affairs, Tianjin 300191, China
[c] Department of Soil Quality, Wageningen University, Wageningen, the Netherlands
[d] College of Natural Resources and Environment, South China Agricultural University, Guangzhou 510642, China

HIGHLIGHTS

- DOM gradually released from biochar (BC) and swine manure (SM) enhanced transport of ferrihydrite nanoparticles (FHNPs).
- Aged BC and SM with large surface roughness manure inhibit FHNPs transport.
- Regulation of BC and SM application avoid contaminants co-transport with FHNPs.

GRAPHICAL ABSTRACT

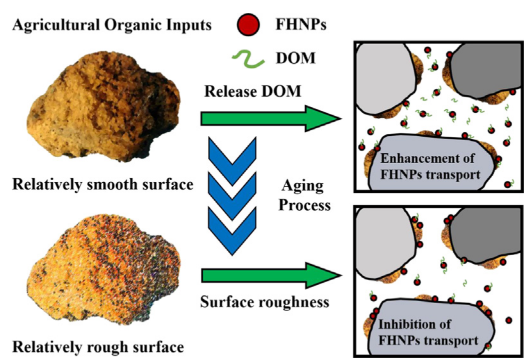

ARTICLE INFO

Article history:
Received 9 January 2020
Received in revised form 18 February 2020
Accepted 18 February 2020
Available online 20 February 2020

Editor: Fang Wang

Keywords:
Biochar
Swine manure
Aging
Ferrihydrite nanoparticles
Transport

ABSTRACT

Organic matter effectively regulates nanoparticles transport. However, little is known about the effect of agricultural organic inputs on the transport of ferrihydrite nanoparticles (FHNPs) during aging. In this study, columns were filled with sand mixed with varying proportions of pristine, water-processing, or alkali-processing biochar or swine manure and used to simulate the release of organic matter and changes in surface roughness of sand grains during field aging. The influence of these factors on FHNPs transport was investigated using column experiments. The dissolved organic matter (DOM) (0.008–24.8 mg L^{-1}) released from agricultural organic inputs decreased the zeta potential of the FHNPs from 30.8 mV to 14.6–-48.9 mV and further caused electrostatic repulsion, osmotic repulsion, and elastic-steric repulsion between FHNPs and mixed sand, thus enhancing FHNPs transport. Ferrihydrite nanoparticles transport increased with increasing content of biochar and swine manure due to the increased amount of DOM. However, with the presence of organic inputs, surface roughness up to a certain degree (the increase in specific surface area up to 4.6 m^2) became the dominant inhibition factor affecting FHNPs transport. After DOM release, agricultural organic inputs decreased the enhancement of FHNPs transport; with the increase input, their rougher surface gradually increased inhibition of FHNPs transport. The strongest FHNPs retention in the alkali-processing biochar (0.2–10%) or swine manure (1–2%) mixed sand columns indicated that fully aged agricultural organic inputs strongly inhibited FHNPs transport. Our findings provided novel insights into the critical influence of agricultural organic inputs and their aging on FHNPs transport, which changed gradually from enhancement to inhibition gradually.

* Corresponding author at: Key Laboratory for Environmental Factors Control of Agro-Product Quality Safety, Ministry of Agriculture and Rural Affairs, Tianjin 300191, China.
E-mail address: majie@caas.cn (J. Ma).
[1] Contributed equally to this study and should be regarded as first joint authors.

https://doi.org/10.1016/j.scitotenv.2020.137440

1. Introduction

Ferrihydrite (FH) is an amorphous iron oxide that is regularly found in the environment as a colloid. Because of the small size of its individual nanocrystals, ferrihydrite nanoparticles (FHNPs) readily transport through porous media. Ferrihydrite nanoparticles transport is influenced by several factors, including pH, ionic strength (IS), and humic acid (HA) (Liao et al., 2017; Ma et al., 2018a; Ma et al., 2018b; Tosco et al., 2012). Ferrihydrite nanoparticles transport increases drastically due to electrostatic repulsion at a pH level greater than 8.2–8.7 (Kosmulski, 2009; Mamindy-Pajany et al., 2011). Our previous studies suggested the moderate FHNPs transport at a neutral pH (Ma et al., 2018a; Ma et al., 2018b). Moreover, FHNPs exhibit high mobility at low ionic strength, while its mobility significantly decreases with increasing salt concentration (Tosco et al., 2012). Humic acid, is a stable component of organic matter in soil (Hemati et al., 2012), can be easily absorbed onto FHNPs, and regulates the surface chemistry and adhesion-transport properties of the particles (Ma et al., 2018b; Wang et al., 2013). Because HA protrudes beyond the Stern layer of the nanoparticle after adsorption (Weng et al., 2006), it has great advantages for influencing FHNPs transport compared with low-molecular-weight organic matters. The HA enhances FHNPs transport at high concentrations (~10–13 mg C L^{-1}), whereas at a low concentration (3 mg C L^{-1}) it can inhibit FHNPs transport (Liao et al., 2017; Ma et al., 2018b). Nevertheless, the size and morphology of HA at different pH levels are crucial to controlling the distance of FHNPs transport. At a neutral pH, chain-shaped HA colloids readily enhance FHNPs transport compared with granular-shaped HA colloids (Ma et al., 2018b).

Ferrihydrite can adsorb pollutants such as As, Pb, Cu, Zn, and Cd due to its extremely high surface area and abundant adsorption sites (Karapinar, 2016; Ma et al., 2018a; Novikov et al., 2006; Tiberg and Gustafsson, 2016). It is claimed that surface groups of FH can induce ligand exchange with oxyanions, e.g., arsenate (AsO_4^{3-}), forming stable ≡Fe-O-As species on the mineral surface (Fendorf et al., 1997; Guo et al., 2013). In most cases, FHNPs disperse in water and transport for long distances in soil or aquifers, which facilitates contaminants transport (Fritzsche et al., 2011; Ma et al., 2018a). Therefore, a good understanding of geochemical behavior of FHNPs, especially under the influence of organic matter, is required.

Biochar and livestock manure are both sustainable, environmentally-friendly, and economical soil amendments to increase soil fertility and crop yield (Antonious, 2018). Biochar is a carbonaceous material synthesized through the pyrolysis/carbonization of wood, manure, or other biomass that can provide a maximum bioenergy output of 8.7 mJ·kg^{-1} with an intermediate yield of 35% biochar (Ahmad et al., 2014; Woolf et al., 2010). When applied to soils, biochar can greatly enhance the pH (for acidic and neutral soils), cation exchange capacity (CEC), nitrogen cycling, water retention, carbon sequestration, microbial activity, and contaminant adsorption of soils (El-Naggar et al., 2018; Liu et al., 2018; Shaaban et al., 2018). The amount of livestock manure produced annually in 12 major livestock-producing countries was 9 billion tons (He et al., 2016). Livestock manure is the largest source of organic fertilizer and can enhance the production of cereals, beans, and oilseeds by increasing N, P, K, and organic matter content in soil (Choudhary et al., 2016). Additionally, similar to biochar, the surface of organic matter in manure has C-, O-, and N-containing surface functional groups with negative charge, and both biochar and livestock manure can act as passivators, in which they absorb or complex heavy metal cations (e.g., Cd, Cu, and Pb) (Bashir et al., 2018; Liang et al., 2017; Meng et al., 2014).

In principle, both biochar and livestock manure can influence the mobility of mineral colloids via modifying the surface properties of colloids as well as the solid matrix. On one hand, the organic matter released from biochar and manure can adsorb to the surface of colloids. Although carbon in biochar is more stable in soil than that in other organic amendments, such as compost and manure, because of its condensed aromatic structure (Awad et al., 2013; Jeffery et al., 2011; Song and Guo, 2012), with weathering, some biochar suffers from oxidation and hydration and is converted into a material with operationally defined properties similar to HA (Hiemstra et al., 2013). Livestock manure contains a large amount of soluble organic carbon, which can be rapidly released (Clark et al., 2007). During mineralization, microbial oxidation takes place within this process, and this can produce a large amount of humus (Hadas et al., 1996). The humic acid contained in biochar and manure can be extracted by washing with alkali (Demirbas, 2005; Jin et al., 2018). On the other hand, the porous structure of biochar and manure presents favorable attachment hotpots for mineral particles (Lin et al., 2012), which may inhibit the transport of colloidal particles.

Consequently, the application of biochar and livestock manure is likely to influence FHNPs transport due to the changes in the physicochemical properties of soil. However, the effects of these agricultural organic inputs on FHNPs transport during their aging process remain obscure. This study systematically investigated the effects of wheat straw biochar and swine manure on FHNPs transport, which focus is placed on the gradual leaching of organic matter and increase in the specific surface area after application to soil, which were simulated by water- and alkali-processing materials. Ferrihydrite nanoparticles transport was assessed by monitoring the breakthrough curves (BTCs) in column experiments. A nanoparticle transport model was used to evaluate the transport rule of FHNPs (Bradford et al., 2003) and the energy interaction between nanoparticles and solid phases are revealed with the extended Derjaguin–Landau–Verwey–Overbeek (XDLVO) theory (Derjaguin and Landau, 1993; Verwey and Overbeek, 1947; Wang et al., 2013). The outcome of this study can improve our understanding of the fate and mobility of FHNPs in agricultural environments. It also can serve as a guide for selecting the appropriate input amounts and application timing of biochar and swine manure in agricultural practices.

2. Materials and methods

2.1. Preparation and characterization of agricultural organic inputs

The biochar was produced from commercial wheat straw at 300 °C. The swine manure was collected from rural areas in Tianjin, China. The dry biochar and swine manure were ground into powder and passed through 0.425 mm nylon sieves and labeled as BC and SM, respectively. The BC and SM were washed using Milli-Q water by shaking repeatedly until their electric conductivities (ECs) were less 50 μS cm^{-1} and 200 μS cm^{-1}, respectively. These two materials were labeled as water-processing biochar (BC-W) and water-processing swine manure (SM-W), respectively to simulate the gradual leaching of dissolved organic matter (DOM) and soluble ions from agricultural organic inputs after their application to soil. In order to simulate the gradual leaching of hydrolyzable organic matter (e.g., HA) and soluble ions from the two kinds of agricultural organic inputs, biochar was first added to 3 M HNO_3 (1:5 m/V), which was heated in a water bath at 85 °C for 24 h to accelerate aging (Hiemstra et al., 2013). Subsequently, after rinsing with Milli-Q water by shaking twice, precipitates were digested using 1 M NaOH (1:5 m/V) by shaking four times (for 24 h each time) to remove humus. Finally, the precipitates were repeatedly washed using Milli-Q water until the EC was less than 50 μS cm^{-1}. The obtained material was as alkali-processing biochar (BC-A). Swine manure was directly digested using 1 M NaOH (1:5 m/V) by shaking four times (for 24 h each) to remove humus and then washed with Milli-Q water until its EC was less than 200 μS cm^{-1}. The obtained material was labeled as alkali-processing swine manure (SM-A).

The properties of the pristine (BC, SM), water-processed (BC-W, SM-W) and alkali-processed (BC-A, SM-A) materials were characterized. The pH and EC were measured in suspensions of a solid-to-water ratio of 1:5 using a multiple parameter meter (SevenExcellence, Toledo). The specific surface area was measured with a specific surface area analyzer (Autosorb-1-C, Quantachrome). Porosity and porosity distribution were measured using an automated mercury porosimeter size analyzer (AutoPore IV 9510, Micromeritics). The capacity of DOM release and the fluorescence excitation–emission matrices (EEMs) were measured in water extractions (solid/water ratio of 1: 10 (m/V)) of the materials using a total organic carbon (TOC) analyzer (Aurora 1030C, OI Analytical) and spectro-fluorometer (FluoroMax-4, Horiba), respectively, after filtering using a 0.45 μm filter. The determination parameters of specific surface area, porosity, porosity distribution, and fluorescence EEMs are listed in Supporting materials S1.

2.2. Ferrihydrite nanoparticles

Ferrihydrite was composited by titrating dissolved $Fe(NO_3)\cdot 9H_2O$ (Sinopharm Chemical Reagent Co. Ltd.) with NaOH to pH 7.5 (Jia et al., 2007). The X-ray diffraction pattern of the solid, verifying the synthesized FH, has been shown in a previous study (Ma et al., 2018b). Suspensions of FHNPs were prepared by adding 0.4 g FH to 400 mL Milli-Q water. The suspension was homogenized by stirring and sonicated for 60 min. After settling for 24 h, the suspension was recovered by siphoning and used immediately after preparation. The transformation of FHNPs did not occur over a short time (Ma et al., 2018a; Ma et al., 2018b). The concentrations of FHNPs were determined by measuring the Fe content using atomic absorption spectroscopy (AAS, AAnalyst 900T, PerkinElmer) after dissolving with 6 M HCl.

2.3. Column experiments

Column experiments were performed in 10-cm-long glass chromatographic columns with an inner diameter of 1.5 cm. Quartz sand (Sinopharm Chemical Reagent Co. Ltd., with an average particle size of 337.5 μm) was cleaned by dipping in 6 M HCl for at least 24 h, followed by rinsing with Milli-Q water repeatedly. The columns were wet packed with quartz sand or quartz sand mixed with agricultural organic inputs. Similar to the heterogeneous mixing of agricultural organic inputs in agricultural applications, varying BC (0.2–10%) or SM (0.2–2%) levels were used to simulate environmental conditions. The filler mixture ratios are listed in Table 1. The effective porosity and bulk density of the packed sand were 0.45 ± 0.02 $cm^3\cdot cm^{-3}$ and 1.43 ± 0.05 $g\cdot cm^{-3}$, respectively for all treatments. After packing, the columns were pre-conditioned with around 15 pore volumes (PVs) of 1 mM NaCl in Milli-Q water using a peristaltic pump (BT-100 1F, Longer) in the up-flow mode. All column experiments were performed at a common soil pH (6.0), and 10 PVs of FHNPs in 1 mM NaCl were injected into the columns, followed by elution with 5 PVs of 1 mM NaCl at pH 6.0 at a constant Darcy velocity of 0.568 $cm\cdot min^{-1}$.

The FHNPs concentrations in the effluent were measured at each PV by AAS after dissolving with 6 M HCl. Concentrations of DOM in the effluent were measured using a TOC analyzer. The particle size and zeta potential of FHNPs and the zeta potential of mixed sand and agricultural organic inputs were measured using a dynamic light scattering analyzer (Zetasizer Nano ZS, Malvern). Following the completion of transport experiments, the sand in the columns was divided into four 2.5-cm-length layers to analyze FHNPs retention by extracting 0.1 g dried filler with 0.5 mL 6 M HCl. The deposition of FHNPs at the entrance of the column (0–2.5 cm) in the treatments with high proportions of agricultural organic inputs (10% BC/BC-W/BC-A and 2% SM/SM-W/SM-A), and the relative element contents were observed with scanning electron microscopy (SEM) with a Zeiss Merlin Compact (at 15 kV) and energy dispersive spectroscopy (EDS) (OxfordX-MAX, Zeiss). The morphology of different agricultural organic inputs was observed simultaneously.

2.4. Transport model

A conservative tracer can check the hydraulic characteristics, including the longitudinal dispersity, of the columns before the nanoparticle transport experiments. A Br^- solution was transported into the column. Effluent Br^- concentration was determined using ion chromatography (ICS-900, Dionex Thermo Fisher). The trace results are shown in Fig. S1 and Table S2.

The transport data were simulated with the nanoparticle transport model which included two-site kinetic retention to describe the nanoparticle transport and retention in the column experiments (Bradford et al., 2003; Yu et al., 2013). For the first kinetic Site-1, the time-dependent retention is taken into account, assuming reversible retention using first-order attachment (k_{1a}) and detachment (k_{1d}) coefficients. For the second kinetic Site-2, depth-dependent retention is considered, assuming irreversible retention using a first-order retention coefficient (k_{2a}), and a depth-dependent blocking function with a Langmuirian approach accounting for maximum nanoparticle content

Table 1
Zeta potential and particle size of the collector and FHNPs (n = 3), released DOM and IS in different columns with mixed ratios of agricultural organic inputs.

Column	Zeta potential of the collector (mV)	Zeta potential of FHNPs[a] (mV)	Particle size of FHNPs (nm)	Released DOM[b] (mg L^{-1})	IS[c] (mM)
Sands	−36.7 ± 0.79	30.8 ± 0.98	181.3 ± 2.8	–	1.00
0.2% BC	−45.5 ± 1.31	−37.3 ± 0.51	174.5 ± 3.2	0.05	1.01
1% BC	−60.7 ± 1.78	−37.2 ± 0.90	181.3 ± 3.0	0.31	1.06
5% BC	−64.9 ± 2.57	−37.5 ± 0.58	184.0 ± 3.5	1.66	1.31
10% BC	−65.2 ± 3.52	−38.3 ± 5.83	210.7 ± 1.0	3.27	1.64
0.2% BC-W	−40.8 ± 0.37	−26.5 ± 0.98	193.3 ± 40.5	0.008	1.00
1% BC-W	−39.6 ± 1.06	−27.2 ± 0.52	192.6 ± 6.0	0.051	1.00
5% BC-W	−47.4 ± 1.40	−29.4 ± 0.26	186.0 ± 5.2	0.24	1.00
10% BC-W	−44.0 ± 0.83	−34.7 ± 6.95	192.9 ± 2.4	0.64	1.00
0.2% BC-A	−37.9 ± 0.84	14.6 ± 0.60	240.9 ± 7.8	0.009	1.00
1% BC-A	−36.7 ± 0.86	−4.0 ± 0.12	1217.0 ± 63.1	0.038	1.00
5% BC-A	−35.3 ± 1.93	−17.8 ± 0.51	690.6 ± 4.1	0.22	1.00
10% BC-A	−34.0 ± 2.12	−24.2 ± 0.74	310.5 ± 6.3	0.46	1.00
0.2% SM	−36.3 ± 0.68	−37.5 ± 0.37	192.3 ± 3.3	2.58	1.01
1%SM	−35.4 ± 0.19	−42.3 ± 0.29	196.3 ± 2.8	14.1	1.05
2% SM	−34.1 ± 0.60	−48.9 ± 0.34	199.0 ± 6.6	24.8	1.12
0.2% SM-W	−36.5 ± 0.66	−21.7 ± 0.19	199.5 ± 3.5	0.16	1.00
1% SM-W	−34.5 ± 0.63	−22.6 ± 0.61	195.2 ± 2.7	1.25	1.00
2% SM-W	−34.0 ± 4.81	−24.5 ± 0.61	217.4 ± 6.7	1.71	1.00
0.2% SM-A	−36.4 ± 0.39	−16.1 ± 0.22	219.0 ± 20.9	0.064	1.00
1% SM-A	−31.2 ± 0.05	−17.9 ± 0.76	221.8 ± 3.6	0.28	1.00
2% SM-A	−30.7 ± 0.62	−19.8 ± 0.31	198.4 ± 4.5	0.53	1.00

[a] The zeta potential of FHNPs mixed with DOM released by agricultural organic inputs.
[b] DOC released by agricultural organic inputs in the effluent.
[c] Total IS is the sum of the background IS and IS released by agricultural organic inputs.

attached on Site-2 (S_{max2}). Detailed equations and parameters are exhibited in Supplementary material S4.

2.5. XDLVO theory

The representative Derjaguin-Landau-Verwey-Overbeek (DLVO) theory performs a function in calculating the total nanoparticle-sand interaction energy by adding Lifshitz-van der Waals (LW) to electrical double layer (EDL) interactions, whereas the extended DLVO (XDLVO) theory includes two additional repulsive interactions, i.e. osmotic repulsion (OSM) and elastic-steric repulsion (ELAS) interaction energies, which is used to determine the total interaction energy in the presence of DOM (Phenrat et al., 2008; Wang et al., 2015). Details of the XDLVO theory and operative equations are presented in Supplementary material S5.

3. Results and discussion

3.1. Physicochemical properties of agricultural organic inputs

Due to the leaching of base cations (Shi et al., 2012), the pH values of BC-W (8.3) and BC-A (8.4) were lower than that of BC (10.1) (Fig. 1a). The SM and SM-W had neutral pH values of 7.4 and 6.7, respectively (Fig. 1a). However, the pH of SM-A increased after processing due to the increase in ammonia (Kim et al., 2012). The ECs of BC-W (48.4 $\mu s \cdot cm^{-1}$) and BC-A (43.6 $\mu s \cdot cm^{-1}$) were much lower than that of BC (6192.8 $\mu s \cdot cm^{-1}$). For swine manure, the initial level and the decrease in EC after pretreatment were lower than that of biochar (Fig. 1b).

The pore size distributions of the biochar mainly ranged from 10 μm to 100 μm, whereas those of the swine manure were wider, ranging from 1 μm to 300 μm (Fig. S2). Although the porosity of BC (76.5%) and SM (65.2%) was basically stable, their pore size distributions changed significantly with the treatments (Figs. 1c and S2). The specific surface area of the BC used in this study was low (2.1 $m^2 g^{-1}$). This value is similar to the specific surface area of biochar produced from wood or grass at 100–300 °C (1.6–4.5 $m^2 g^{-1}$) in previous studies (Keiluweit et al., 2010). The specific surface area of biochar and swine manure increased after water- and alkali-processing (Fig. 1c). Water-processing slightly decreased the pore size of materials (Fig. S2) and increased their specific surface area (from 2.1 $m^2 g^{-1}$ to 5.3 $m^2 g^{-1}$ and from 8.1 $m^2 g^{-1}$ to 8.9 $m^2 g^{-1}$ for biochar and swine manure, respectively) (Fig. 1c). The alkali-processing had a greater impact. For biochar, corrosion from the strong alkali increased the amount of ~10–20 μm macropores of BC-A, thus increased its specific surface area (Jiang et al., 2002). For swine manure, the interactions between NaOH and the carbon matrix dissolved and degraded the amount of organic matter (Wang et al., 2019), which was mainly manifested as a significant increase in the specific surface area (from 8.0 $m^2 g^{-1}$ to 14.2 $m^2 g^{-1}$) and the change in the pore distribution (Fig. S2). These changes are comparable to the aging effect on organic inputs in agricultural soil. Biochar aged for 1–1.3 years had a highly porous surface compared with the pristine sample (Ren et al., 2018). The structure of swine manure formed particles fragmented during its degradation in soil (Ge et al., 2015).

Water- and alkali-processing procedures removed DOM and HA from the BC and SM (Kalbitz et al., 2000). Biochar and SM contained varying levels of DOM, and the former contained far less than the latter (Fig. 1d). The lowest amounts of released DOM and coarsest surfaces (Figs. 1d and S3) were observed in the BC-A and SM-A.

3.2. Effect of biochar on FHNPs transport

The mobility of FHNPs was evaluated using transport experiments in sand or BC-, BC-W-, and BC-A-mixed sand columns. The observed and simulated the breakthrough curves (BTCs) of FHNPs transport are shown in Fig. 2. The fitted parameters of the nanoparticle transport model are presented in Table S3. Total FHNPs recovery ranged from 87.0% to 117.9% at different additive amounts (Table S3). The recovery of FHNPs from the effluent and column represent the transport and deposition of the nanoparticles, respectively (Table S3).

When FHNPs existed individually, their gradual breakthrough showed moderate transport capacity, due to their nanoscale particle size (Fig. 2a). At a low additive amount of BC (0.2%), although larger change in the zeta potential of sand and FHNPs (from −36.7 mV to −45.5 mV and from 30.8 mV to −37.3 mV, respectively) were observed (Table 1), the low amount of DOM released decreased the positive potential of FHNPs close to 0 at the inlet during the initial contact between

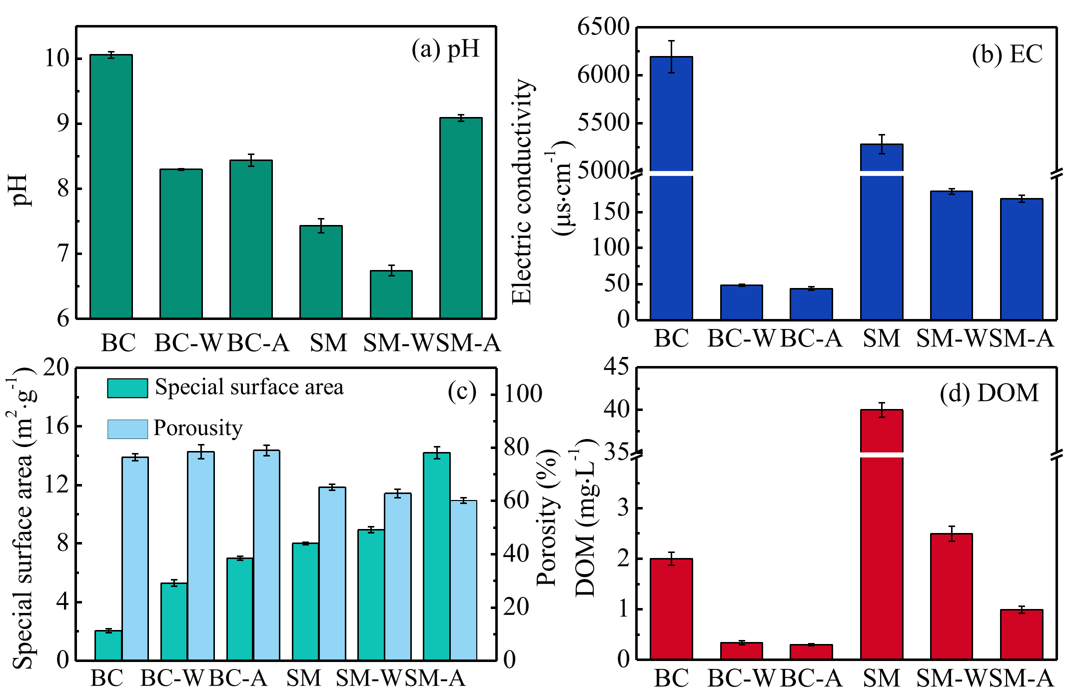

Fig. 1. The pH, EC, specific surface area, and DOM (DOC) of BC and SW with and without different treatments.

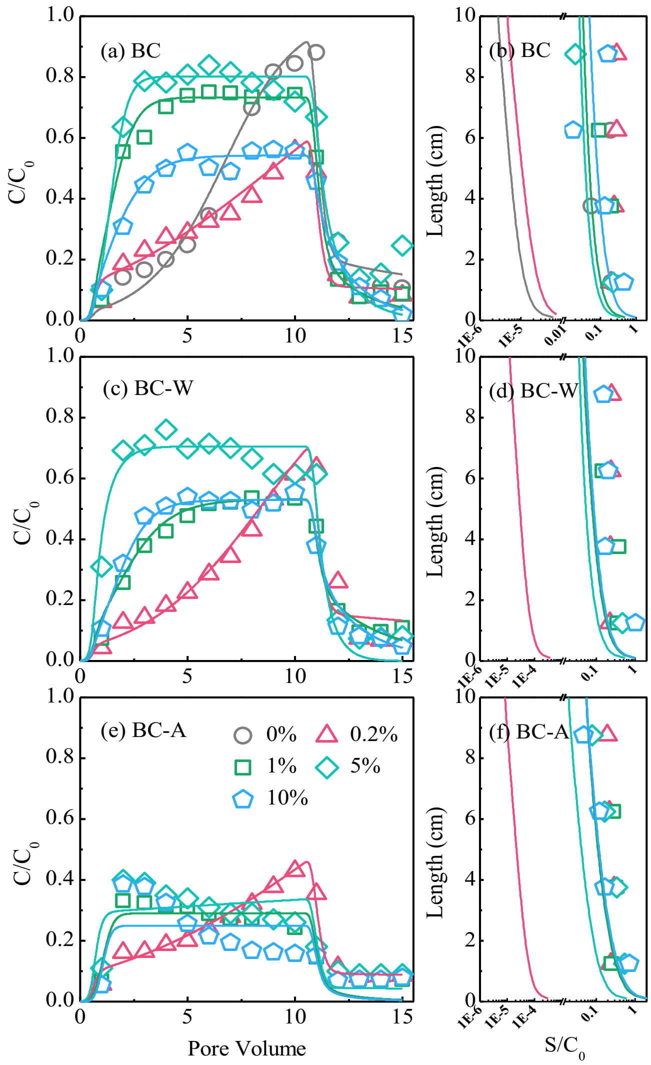

Fig. 2. Breakthrough curves (a, c, and e) and RPs (b, d, and f) of FHNPs in columns with different quantities of BC (a and b), BC-W (c and d) and BC-A (e and f) at pH 6.0. The FHNPs RPs were plotted as the initial nanoparticle concentration normalized (nanoparticle retention in the sand columns S_r divided by initial nanoparticle concentration) as nanoparticle retention per gram of dry sand as a function of distance from the column inlet. Symbols and solid lines show the observed data and simulation fitting, respectively.

DOM and FHNPs. This low DOM concentration may decrease FHNPs transport (Fig. 2a) (Liao et al., 2017). When the addition of BC increased to 1–5%, the increase in breakthrough, FHNPs recovery from the effluent, and k_{1d}/k_{1a} values (Fig. 2a and Table S3) indicated readily FHNPs transport compared with treatments without BC. The high DOM concentrations were attributed to the increase in the negative zeta potential of the mixed sands and FHNPs with increasing quantity of BC (Table 1), which increased the electrostatic repulsion between them (Ma et al., 2018b; Philippe and Schaumann, 2014). However, when the BC content was increased to 10%, FHNPs transport decreased compared with that of 1% and 5% BC (Fig. 2a). In this case, we speculated that the surface roughness (specific surface area) may play a more significant role in FHNPs retention (Shen et al., 2011; Torkzaban and Bradford, 2016). The effect of DOM on FHNPs transport did not increase continuously with the increase of DOM due to the adsorption saturation of DOM on FHNPs, as confirmed by the basically stable zeta potential of the FHNPs (Table 1). We further speculated that the increase in retention caused by the increase in surface roughness was beyond the enhancement of electrostatic repulsion due to the adsorption of DOM. The maximized release of ions also inhibited FHNPs transport (Liu et al., 2019; Tosco et al., 2012).

The effect of BC-W on FHNPs transport was similar to that of BC. However, due to the less amount of DOM released (Fig. 1d) and consequently less decrease in the negative zeta potential of FHNPs and mixed sands (Table 1), FHNPs transport was more inhibited compared with that of BC treatment (Fig. 2a and c). A reduced breakthrough of FHNPs with decreases in DOM concentrations has been observed in previous studies (Liao et al., 2017; Ma et al., 2018a; Ma et al., 2018b). Since the difference in specific surface area between BC (2.1 $m^2\ g^{-1}$) and BC-W (5.3 $m^2\ g^{-1}$) was relatively large (Fig. 1c), the surface roughness of the collector also contributed to the decrease in FHNPs transport. For BC-A, although porosity was basically stable, the porosity distribution and specific surface area changed significantly (Figs. 1c and S2a). These changes, especially the creation of more macropores of BC-A (10–20 μm) (Fig. S2a), were conducive to FHNPs retention (Fallahianbijan et al., 2017; Tosco et al., 2012). Moreover, the least amount of DOM released by BC-A among the treatments could barely enhance the FHNPs transport. Therefore, BC-A inhibited FHNP transport and the influence increased with increasing additive amounts of BC-A (Fig. 2e). The increasing FHNPs retention rate over time occurred due to the ripening behavior (Fig. 2e). The more pronounced retention near the column inlet caused "dead-ends" in the collector pores and, consequently, increased the physical strain. The k_{1d}/k_{1a} values in BC-W and BC-A mixed columns first increased and then decreased (Table S3), consistent with their transport characteristics.

The retention profiles (RPs) of FHNPs in the porous media were used to evaluate FHNPs deposition. In this study, although deviations between the observed data and simulated FHNPs retention fittings existed due to that the breakthrough plateaus were not reached (sand column and 0.2% BC-, BC-W-, and BC-A-mixed sand columns), FHNPs deposition typically displayed similar characteristics in different columns. A hyperexponential retention profile with greater retention in the column inlet (0–2.5 cm) and decreasing retention with column depth was observed (Fig. 2b, d, and f).

3.3. Effect of swine manure on FHNPs transport

To compare the effect of swine manure on FHNPs transport with that of biochar, we also carried out transport experiments in columns of sand mixed with SM, SM-W, and SM-A. The observed and simulated results of FHNPs transport are shown in Fig. 3. The fitted parameters are presented in Table S4. Like the various processing biochar-mixed sand column experiments, FHNPs recoveries in the effluent and columns were roughly consistent with the effects of SM, SM-W, and SM-A and their quantities on FHNPs transport. Total FHNPs recoveries were between 84.2% and 110.0%, indicating credible experimental data.

Effects of SM, SM-W, and SM-A on FHNPs transport varied with the amount added. Because SM can release more DOM than biochar (Fig. 1d), a low swine SM (0.2%) clearly enhanced FHNPs transport compared with that of 0.2% biochar (Figs. 2a and 3a). When the amount of SM increased from 0.2% to 1%, the greater DOM released by the SM loaded onto FHNPs, which increased their negative zeta potential (Table 1) to create stronger electrostatic repulsions against SM-mixed sand. This high DOM release also increased FHNPs transport in 1% SM compared to that in 1% BC (Figs. 2a and 3a). Ferrihydrite nanoparticles transport decreased when at 2% SM (Fig. 3a). This was partly attributed to the lower negative zeta potential of swine manure (−31.8 mV) compared with sand (−36.7 mV), which decreased the negative zeta potential of the collector (−34.1 mV) (Table 1 and S1). However, the surface roughness, macropores, and ions of SM may primarily hamper FHNPs transport.

As with the influence of biochar, the enhancement of FHNPs transport gradually decreased with processing (Fig. 3) due to the decrease in DOM released and increase in the specific surface area. However, low content (0.2%) SM-W and SM-A always enhanced FHNP transport

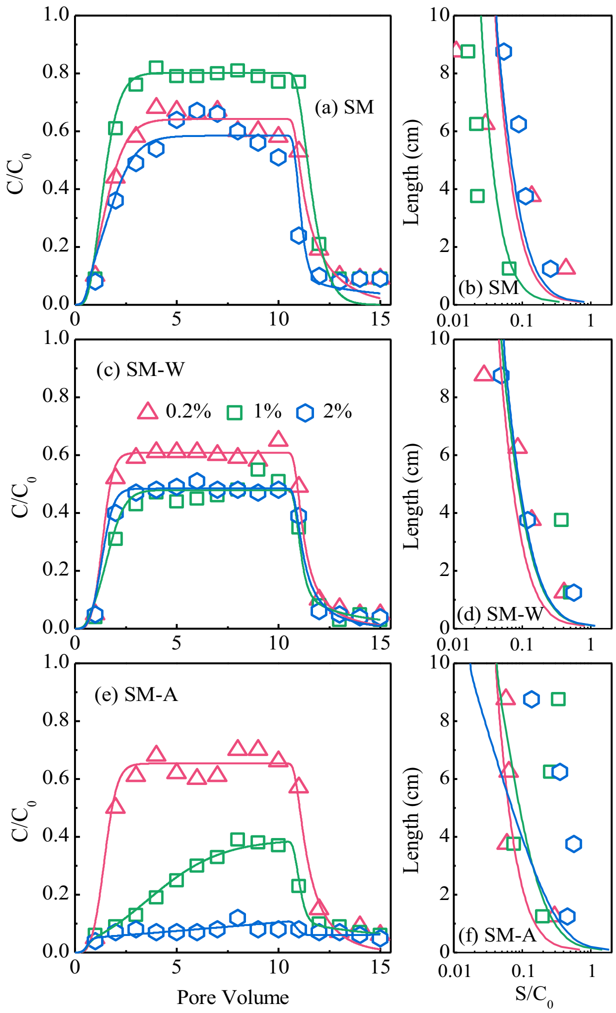

Fig. 3. Breakthrough curves (a, c, and e) and RPs (b, d, and f) of FHNPs in columns with different quantities of SM (a and b), SM-W (c and d) and SM-A (e and f) at pH 6.0. The FHNPs RPs were plotted as the initial nanoparticle concentration normalized (nanoparticle retention in the sands columns S_r divided by initial nanoparticle concentration) as nanoparticle retention per gram of dry sand as a function of distance from the column inlet. Symbols and solid lines show the observed data and simulation fitting, respectively.

(Fig. 3), as the additions of minimal SM-W or SM-A did not significantly increase the roughness of the collector. The increases in the specific surface area were 0.51 and 0.82 m^2, respectively. Therefore, this did not offset the enhancement caused by relatively large amount of DOM released. The inhibition effect gradually predominated with increasing amount of SM-W and SM-A (Fig. 3c and e). Especially for SM-A, the relatively large specific surface area and low DOM release capacity led to obvious inhibition of FHNP transport when 2% SM-A was added in the columns (Fig. 3e). The k_{1d}/k_{1a} values in the SM-, SM-W-, and SM-A-mixed column showed firstly an increase followed by a decrease, little change, and gradual decrease, respectively (Table S4), consistent with their transport characteristics. The surface roughness of swine manure caused by macropores from substances with vascular bundle structures (Duan et al., 2011) increased favorable retention sites for FHNPs (Shen et al., 2011). Moreover, its relatively high IS may have contributed to FHNPs retention (Chen et al., 2017). An analogous phenomenon occurred when 10% BC was added. The increase in specific surface area derived from 2% SM (4.6 m^2) was high and slightly lower than that of 10% BC (6.0 m^2), indicating that a certain level of surface roughness was the key factor of FHNPs retention.

In the presence of swine manure with different treatments, FHNP deposition displayed a hyperexponential RP (Fig. 3b, d, and f) similar to the biochar-mixed sand columns (Fig. 2b, d, and f), showing significant depth-dependency. The observed data and simulated fitting of FHNPs retention roughly matched for the SM- and SM-W-mixed columns. For the SM-A mixed columns, the high FHNPs retention in the porous medium led to some FHNPs deposition away from the inlet and further resulted in deviations in FHNPs retention between the observed data and simulation fittings.

3.4. Effect of DOM on interaction energy between FHNPs and sand

The XDLVO theory was used to calculate the interaction energy between FHNPs and sand in the presence of agricultural organic inputs. The XDLVO calculation results shown in Fig. 4 qualitatively explain FHNPs transport trends. The parameters used in this calculation are listed in Table 1 and Supplementary material S5. The presence of DOM caused osmotic repulsion (OSM) and elastic-steric repulsion (ELAS) between the FHNPs and sand (Wang et al., 2015).

There was no primary energy barrier between the FHNPs and pure quartz sand, and the interaction energy between them was always less than 0 (Fig. 4a). In this case, FHNPs readily deposited on the sand. The primary energy barriers between the FHNPs and mixed sand increased with the amount of changing BC from 0% to 5% (from 0 kT to 252.2 kT) (Fig. 4a) consistent with their transport characteristics (Fig. 2a). These results indicated that the DOM released by BC and loaded on FHNPs enhanced transport due to electrical double layer repulsion (EDL), OSM, and ELAS. Previous studies have also reported that the presence of organic matter changed the surface characteristics of hydroxyapatite nanoparticles and metal oxide nanoparticles, thereby causing electrostatic repulsion between the particles that maintained their dispersion stability in solution (Keller et al., 2010; Wang et al., 2012). Osmotic repulsion and ELAS significantly enhanced the primary energy barrier between the FHNPs and mixed sand (at ~1–2.5 nm) when the amount of added BC increased from 0.2% to 5% (Fig. 4a). Although the highest primary energy barrier (295.3 kT) was found in the 10% BC-mixed sand column (Fig. 4a), FHNPs transport was slower than that in columns with a BC content of 1% or 5% (Fig. 2a). This inconsistency indicated that another factor, such as the surface roughness, dominated the deposition of FHNPs, consistent with the previous study (Shen et al., 2011; Torkzaban and Bradford, 2016).

Because of the low amount of DOM released by BC-W (Fig. 1d), the negative zeta potential of FHNPs and mixed sand decreased (Table 1). Therefore, the primary energy barriers between the FHNPs and BC-W-mixed sand (118.2–183.8 kT) decreased overall compared with that in BC-mixed sand columns (Fig. 4a and b). The gap between the FHNPs transport and XDLVO results remained at high BC-W quantities (10%) (Figs. 4b and 2c). When the agricultural organic inputs were switched to BC-A, the primary energy barriers between the collectors and FHNPs (0–174.3 kT) further decreased and the deviations in FHNPs transport and XDLVO results were more obvious (Figs. 4c and 2e). Although the primary energy barriers were observed in the 5% and 10% BC-A columns, FHNPs had poor mobility.

In column experiments with different processing swine manure additions, the primary energy barriers between the FHNPs and the collectors were lower than in different processing biochar columns owing to the relatively small influence of the agricultural organic inputs on the zeta potential of FHNPs and mixed sand (Table 1). Moreover, the values of primary energy barriers gradually decreased during swine manure aging (Fig. 4d, e, and f) due to the decrease in the negative zeta potential of the porous media and FHNPs (Table 1) as a result of the diminishment of DOM (Fig. 1d). For low and moderate additions of SM and SM-W, the XDLVO results were consistent with the observations from column experiments, indicating that FHNPs transport/detachment was regulated by EDL, OSM, and ELAS. Deviations between FHNPs transport and XDLVO results occurred in columns with 2% SM-, 2% SM-W-, 1% SM-A-, and 2% SM-A-mixed sand (Figs. 4f and 3e). Although obvious primary energy barriers between the FHNPs and the collectors were

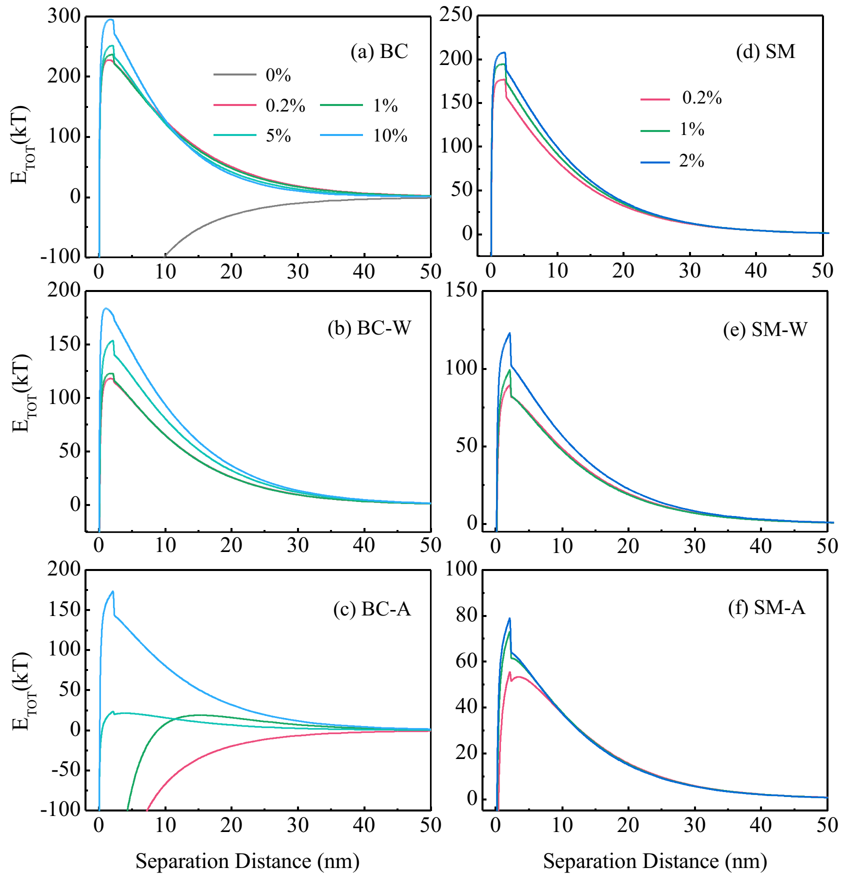

Fig. 4. XDLVO interaction energy between FHNPs and sand in the presence of DOM released by agricultural organic inputs. The interaction energy is expressed in kT, where k is the Boltzmann constant, and T is the absolute temperature in Kelvin.

exhibited, FHNPs showed relatively poor mobility in the presence these additions, which proved our assumption discussed above, i.e., that the relatively high specific surface area of agricultural organic inputs, especially aged materials, counteracted the promoting effect of the released DOM on FHNPs transport, causing an increase in FHNPs retention. The FHNPs transport may change from enhancement to inhibition with the decreasing ability of the agricultural organic inputs to release DOM and their increasing surface roughness during aging in agricultural soil.

Numerous studies have suggested that organic matter can enhance the transport of nanoparticles or colloids (Liao et al., 2017; Ma et al., 2018a; Ma et al., 2018b; Wang et al., 2012; Wang et al., 2013). The high molecular weight-DOM (e.g. humic substances) exhibited higher adsorption capacities and affinities than the low molecular weight-DOM (Xu et al., 2019). The HA particles, a representative high molecular weight-DOM, as adsorbed were shown to protrude beyond the Stern layer of the nanoparticle (Weng et al., 2006) and thus significantly changed the electrical properties of nanoparticle. Hence, the enhancement of HA on nanoparticle transport was much greater than that of low-molecular-weight organic acid and fulvic acid, which were located in the Stern layer after adsorption. Based on these observations, we calculated the excitation–emission spectra and humification index for DOM released by different agricultural organic inputs (Supplementary material S8). The fluorescence intensity of the humic-like area (the region of $E_x = 250–420$ nm, $E_m = 380–520$ nm) and humification index of biochar and swine manure decreased (Fig. 5) after water- and alkali-processing due to organic dissolution and the destruction of polycyclic structures (Wei et al., 2014). These results indicated that the decrease in FHNPs transport during the aging of agricultural organic inputs was caused by the superimposed effect of diminishing DOM concentrations and degree of humification. Although the protein-like fraction (the region of $E_x = 250–320$ nm, $E_m = 300–380$ nm) increased after water- and alkali-processing, it had a much smaller impact on FHNPs than humic substances due to its low molecular weight. Even at high DOM concentrations, surface roughness affected the FHNPs deposition. Although many factors, such as straining effect, ripening behavior, and heterogeneity could be conducive to FHNPs retention (Eddy et al., 2014; Farahat et al., 2009; Ma et al., 2018b; Torkzaban et al., 2008; Wang et al., 2015), surface roughness played an important role, which we will discuss with regard to the depositional morphology of FHNPs.

3.5. Depositional morphology of FHNPs

Ferrihydrite nanoparticles deposition in different processing 10% biochar and 2% swine manure columns was observed with SEM and EDS chemical composition analysis. As shown in the characteristics of transport and retention, the FHNPs were readily deposited near the column inlet (0–2.5 cm). In the presence of agricultural organic inputs, although some FHNPs may deposit directly onto the sand, the dots highlighted on the rough surfaces in the SEM images indicated that more FHNPs deposited on the agricultural organic inputs (Fig. 6). Data of EDS showed the coexistence of C (0–71.8%) and Fe (1.2–7.0%) (Fig. 6). The high Fe signals were observed on the nonferrous organic matter also indicated FHNPs retention on biochar and swine manure aged to different stages. Silicon signals in the EDS scanning area were high due to the electron beam scanning into the quartz sand background. The agricultural organic inputs increased the chemical and physical heterogeneity of porous media, which is beneficial for FHNPs retention (Ma et al., 2018a). Although biochar and swine manure

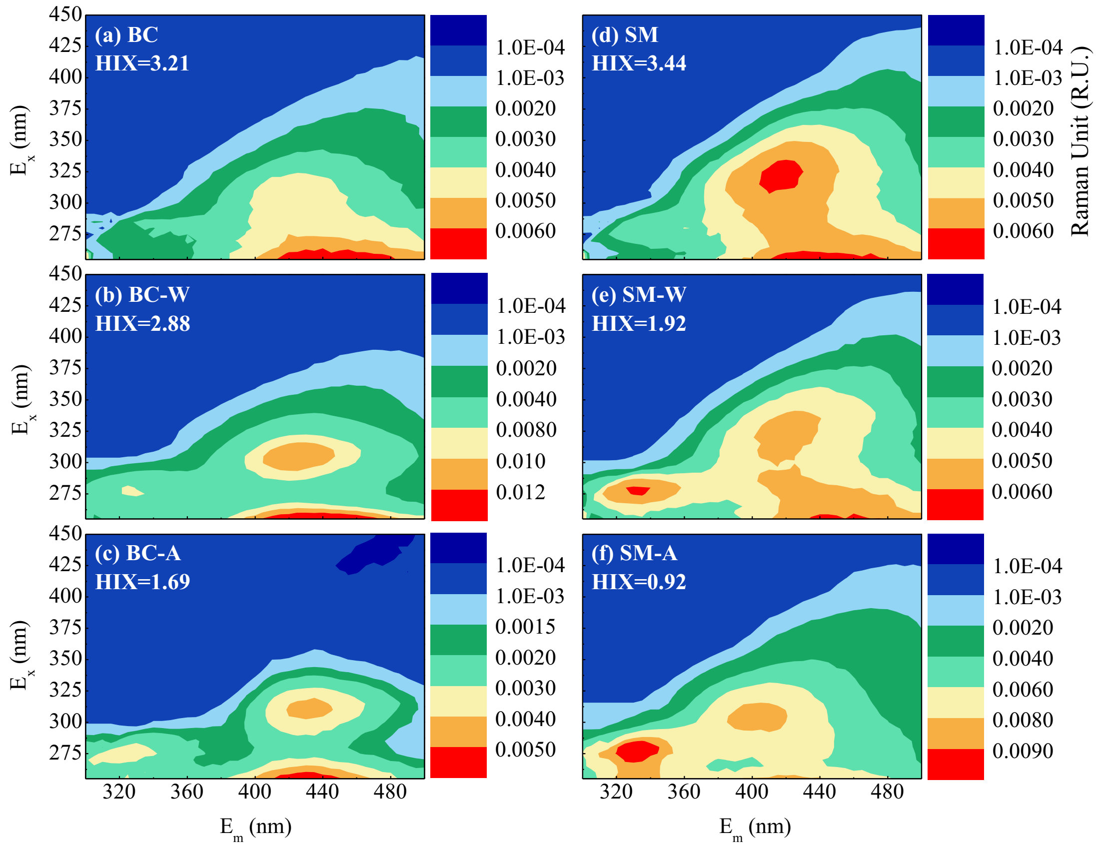

Fig. 5. Excitation-emission spectra and humification index for DOM released by different agricultural organic inputs.

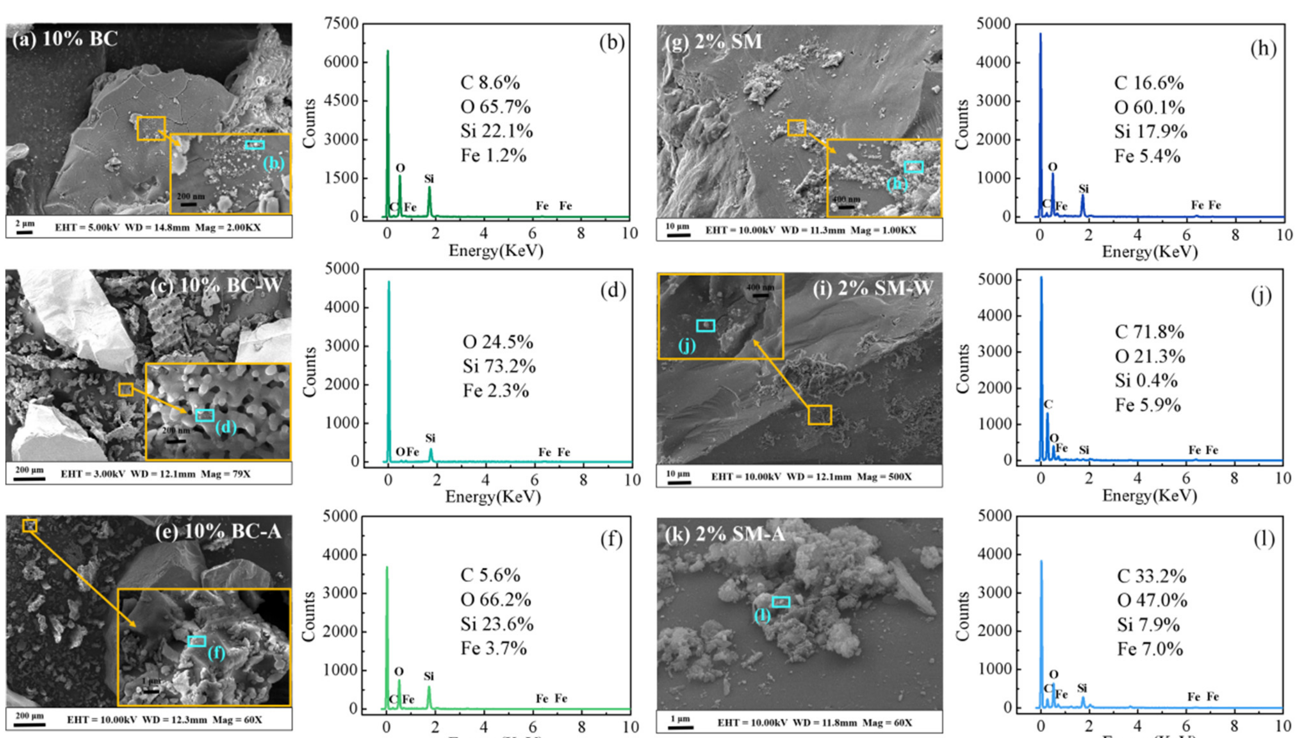

Fig. 6. SEM images of FHNPs deposition on the mixed sands (a, c, e, g, i, and k show BC, BC-W, BC-A, SM, SM-W, and SM-A, respectively) from the 0–2.5 cm layer of columns and the corresponding EDS spectra for regions of FHNPs deposition (b, d, f, h, j, and l).

introduced negative charges in the collectors, which can produce electrostatic attraction to the positively charged FHNPs, the DOM released by the biochar and swine manure also caused the negative charged loading onto FHNPs (Table 1). Therefore, the effect of chemical heterogeneity on FHNPs deposition may be relatively small. Physical heterogeneity may play more important role in FHNPs retention.

Numerous studies have indicated that collector surface roughness promotes colloid or nanoparticle deposition (Bradford et al., 2017; Bradford et al., 2003; Li et al., 2017; Shen et al., 2011; Shen et al., 2012). Roughness fraction and height can induce the primary minimum interactions that cause deposition, even under electrostatically unfavorable conditions (Bradford et al., 2017). Unquestionably, increasing the amount of agricultural organic inputs could increase the roughness fraction and height of porous media. Notably, aging agricultural organic inputs in soils can also increase its roughness fraction. The increasing specific surface area of biochar and swine manure during aging (Fig. 1c) was beneficial to deposition of FHNPs due to continuously formed macropores, mesopores, and slits (Fig. S3). Microscale roughness dramatically altered the lever arms associated with hydrodynamic and adhesive torques (Torkzaban and Bradford, 2016) to the benefit of irreversible attachment of FHNPs in concave regions (Shen et al., 2012).

4. Conclusion

In this study, water- and alkali-processing biochar and swine manure were used to simulate agricultural organic inputs during field aging. Aging was accompanied by an increase in the specific surface area of the particulate organic particles and a decrease in the amount of DOM released. The amount of agricultural organic input and its aging affect FHNPs transport. Pristine agricultural organic inputs released a large amount of DOM, which transformed the zeta potential of FHNPs and caused electrical double layer (EDL), osmotic repulsion (OSM) and elastic-steric repulsion (ELAS) between the FHNPs and mixed sand, increasing FHNPs transport. With decrease of DOM released, the effect of water-processing agricultural organic inputs on FHNPs transport decreased. During further aging, simulated with alkali-processing, inhibition effect on FHNPs transport became dominant. In some cases where the specific surface area of particulate organic matter significantly increased, XDLVO calculation did not explain the transport results well, because the calculations did not consider the physical retention effect. The increase in the amount and aging of agricultural organic inputs in soil increased the roughness fraction and further enhanced FHNPs deposition. Our results suggested that during aging, the effect of agricultural organic inputs on the FHNPs transport gradually shifted from enhancement to inhibition. Although the inhibition effect of aged organic agricultural organic inputs on FHNPs transport was obvious, at the beginning of application, fresh biochar or swine manure could enhance FHNPs transport and further promote the FHNP-assisted transport of pollutants. This work, to our knowledge, is the first study describing the effects of environmental processes of actual agricultural organic inputs on FHNPs transport, in contrast to the existing studies using purified (e.g., HA) or synthesized organic matter. Future research should study the micro-interfacial mechanism of the influence of agricultural organic inputs and their aging on the co-transport and co-deposition of pollutants with nanoparticles or colloids.

CRediT authorship contribution statement

Xiaoyan Qian: Resources, Investigation, Formal analysis, Writing - original draft. **Jie Ma:** Conceptualization, Methodology, Writing - original draft, Funding acquisition. **Liping Weng:** Writing - review & editing. **Yali Chen:** Writing - review & editing. **Zongling Ren:** Writing - review & editing, Funding acquisition. **Yongtao Li:** Writing - review & editing.

Declaration of competing interest

The authors declare that they have no known competing financial interests or personal relationships that could have appeared to influence the work reported in this paper.

Acknowledgments

The study is financially supported by the National Natural Science Foundation of China (No. 41701262), National Key Research and Development Program of China (2017YFD0801003), National Natural Science Foundation of China (Nos. 41601227, and 41771277), Natural Science Foundation of Tianjin City (19JCQNJC08500), Central Public-interest Scientific Institution Basal Research Fund (2019-jbkyywf-mj).

Appendix A. Supplementary data

Supplementary data to this article can be found online at https://doi.org/10.1016/j.scitotenv.2020.137440.

References

Ahmad, M., Rajapaksha, A.U., Lim, J.E., Zhang, M., Bolan, N., Mohan, D., et al., 2014. Biochar as a sorbent for contaminant management in soil and water: a review. Chemosphere 99, 19–33.
Antonious, G.F., 2018. Biochar and animal manure impact on soil, crop yield and quality. Agricultural Waste & Residues pp. 45–67.
Awad, Y.M., Blagodatskaya, E., Ok, Y.S., Kuzyakov, Y., 2013. Effects of polyacrylamide, biopolymer and biochar on the decomposition of 14C-labelled maize residues and on their stabilization in soil aggregates. Eur. J. Soil Sci. 64, 488–499.
Bashir, S., Shaaban, M., Mehmood, S., Zhu, J., Fu, Q.L., Hu, H.Q., 2018. Efficiency of C3 and C4 plant derived-biochar for Cd mobility, nutrient cycling and microbial biomass in contaminated soil. Bulletin of Environmental Contamination & Toxicology 100, 834–838.
Bradford, S.A., Simunek, J., Bettahar, M., van Genuchten, M.T., Yates, S.R., 2003. Modeling colloid attachment, straining, and exclusion in saturated porous media. Environmental Science & Technology 37, 2242–2250.
Bradford, S.A., Kim, H., Shen, C.Y., Sasidharan, S., Shang, J.Y., 2017. Contributions of nanoscale roughness to anomalous colloid retention and stability behavior. Langmuir 33, 10094–10105.
Chen, M., Wang, D.J., Yang, F., Xu, X.Y., Xu, N., Cao, X.D., 2017. Transport and retention of biochar nanoparticles in a paddy soil under environmentally-relevant solution chemistry conditions. Environ. Pollut. 230, 540–549.
Choudhary, M., Bailey, L.D., Grant, C.A., 2016. Review of the use of swine manure in crop production: effects on yield and composition and on soil and water quality. Waste Manag. Res. 14, 581–595.
Clark, G.J., Dodgshun, N., Sale, P.W.G., Tang, C., 2007. Changes in chemical and biological properties of a sodic clay subsoil with addition of organic amendments. Soil Biol. Biochem. 39, 2806–2817.
Demirbas, M.F., 2005. Nitrogenous chemicals from carbon based materials. Energy Explor. Exploit. 23, 215–224.
Derjaguin, B., Landau, L., 1993. Theory of the stability of strongly charged lyophobic sols and of the adhesion of strongly charged particles in solutions of electrolytes. Prog. Surf. Sci. 43, 30–59.
Duan, Y., Xu, M., He, X., Li, S., Sun, X., 2011. Long-term pig manure application reduces the requirement of chemical phosphorus and potassium in two rice-wheat sites in subtropical China. Soil Use & Management 27, 427–436.
Eddy, P., Jacob, T., Johnson, W.P., 2014. Release of colloids from primary minimum contact under unfavorable conditions by perturbations in ionic strength and flow rate. Environmental Science & Technology 48, 9227–9235.
El-Naggar, A., Awad, Y.M., Tang, X.Y., Liu, C., Niazi, N.K., Jien, S.H., et al., 2018. Biochar influences soil carbon pools and facilitates interactions with soil: a field investigation. Land Degrad. Dev. 29, 2162–2171.
Fallahianbijan, F., Giglia, S., Carbrello, C., Zydney, A.L., 2017. Use of fluorescently-labeled nanoparticles to study pore morphology and virus capture in virus filtration membranes. J. Membr. Sci. 536, 52–58.
Farahat, M., Hirajima, T., Sasaki, K., Doi, K., 2009. Adhesion of Escherichia coli onto quartz, hematite and corundum: extended DLVO theory and flotation behavior. Colloids Surf B Biointerfaces 74, 140–149.
Fendorf, S., Eick, M.J., Grossl, P., Sparks, D.L., 1997. Arsenate and chromate retention mechanisms on goethite. 1. Surface structure. Environmental Science & Technology 31, 315–320.
Fritzsche, A., Rennert, T., Totsche, K.U., 2011. Arsenic strongly associates with ferrihydrite colloids formed in a soil effluent. Environ. Pollut. 159, 1398–1405.
Ge, J.Y., Huang, G.Q., Huang, J., Zeng, J.F., Han, L.J., 2015. Mechanism and kinetics of organic matter degradation based on particle structure variation during pig manure aerobic composting. J. Hazard. Mater. 292, 19–26.
Guo, H.M., Ren, Y., Liu, Q., Zhao, K., Li, Y., 2013. Enhancement of arsenic adsorption during mineral transformation from siderite to goethite: mechanism and application. Environmental Science & Technology 47, 1009–1016.

Hadas, A., Kautsky, L., Portnoy, R., 1996. Mineralization of composted manure and microbial dynamics in soil as affected by long-term nitrogen management. Soil Biol. Biochem. 28, 733–738.

He, Z.Q., Pagliari, P.H., Waldrip, H.M., 2016. Applied and environmental chemistry of animal manure: a review. Pedosphere 26, 779–816.

Hemati, A., Alikhani, H.A., Marandi, G.B., 2012. Extractants and extraction time effects on physicochemical properties of humic acid. International Journal of Agriculture Research & Review 2, 975–984.

Hiemstra, T., Mia, S., Duhaut, P.-B., Molleman, B., 2013. Natural and pyrogenic humic acids at goethite and natural oxide surfaces interacting with phosphate. Environmental Science & Technology 47, 9182–9189.

Jeffery, S., Verheijen, F.G.A., van der Velde, M., Bastos, A.C., 2011. A quantitative review of the effects of biochar application to soils on crop productivity using meta-analysis. Agric. Ecosyst. Environ. 144, 175–187.

Jia, Y.F., Xu, L.Y., Wang, X., Demopoulos, G.P., 2007. Infrared spectroscopic and X-ray diffraction characterization of the nature of adsorbed arsenate on ferrihydrite. Geochim. Cosmochim. Acta 71, 1643–1654.

Jiang, X.M., Zheng, C.G., Yan, C., Liu, D.C., Qiu, J.R., Li, J.B., 2002. Physical structure and combustion properties of super fine pulverized coal particle. Fuel 81, 793–797.

Jin, J., Sun, K., Yang, Y., Wang, Z.Y., Han, L.F., Wang, X.K., et al., 2018. Comparison between soil- and biochar-derived humic acids: composition, conformation, and phenanthrene sorption. Environmental Science & Technology 52, 1880–1888.

Kalbitz, K., Solinger, S., Park, J.H., Michalzik, B., Matzner, E., 2000. Controls on the dynamics of dissolved organic matter in soils: a review. Soil Sci. 165, 277–304.

Karapinar, N., 2016. Removal of heavy metal ions by ferrihydrite: an opportunity to the treatment of acid mine drainage. Water Air Soil Pollut. 227.

Keiluweit, M., Nico, P.S., Johnson, M.G., Kleber, M., 2010. Dynamic molecular structure of plant biomass-derived black carbon (biochar). Environmental Science & Technology 44, 1247–1253.

Keller, A.A., Wang, H.T., Zhou, D.X., Lenihan, H.S., Cherr, G., Cardinale, B.J., et al., 2010. Stability and aggregation of metal oxide nanoparticles in natural aqueous matrices. Environmental Science & Technology 44, 1962–1967.

Kim, C.L., Kim, S.R., Kim, H.J., Jeon, S.J., Han, H., Kim, D.K., et al., 2012. Physicochemical changes of swine manure by the treatment of acid and alkali for inactivation of pathogenic microorganisms. Journal of Livestock Housing & Environment 18, 229–234.

Kosmulski, M., 2009. Compilation of PZC and IEP of sparingly soluble metal oxides and hydroxides from literature. Advances in Colloid & Interface Science 152, 14–25.

Li, T.T., Jin, Y., Huang, Y.F., Li, B.G., Shen, C.Y., 2017. Observed dependence of colloid detachment on the concentration of initially attached colloids and collector surface heterogeneity in porous media. Environmental Science & Technology 51, 2811–2820.

Liang, J., Li, X.M., Yu, Z.G., Zeng, G.M., Luo, Y., Jiang, L.B., et al., 2017. Amorphous MnO2 modified biochar derived from aerobically composted swine manure for adsorption of Pb(II) and Cd(II). ACS Sustain. Chem. Eng. 5, 5049–5058.

Liao, P., Li, W.L., Wang, D.J., Jiang, Y., Pan, C., Fortner, J.D., et al., 2017. Effect of reduced humic acid on the transport of ferrihydrite nanoparticles under anoxic conditions. Water Res. 109, 347–357.

Lin, Y., Munroe, P., Joseph, S., Kimber, S., Van Zwieten, L., 2012. Nanoscale organo-mineral reactions of biochars in ferrosol: an investigation using microscopy. Plant Soil 357, 369–380.

Liu, G.C., Zheng, H., Jiang, Z.X., Wang, Z.Y., 2018. Effects of biochar input on the properties of soil nanoparticles and dispersion/sedimentation of natural mineral nanoparticles in aqueous phase. Sci. Total Environ. 634, 595–605.

Liu, J., Louie, S.M., Pham, C., Dai, C., Liang, D.L., Hu, Y.D., 2019. Aggregation of ferrihydrite nanoparticles: effects of pH, electrolytes, and organics. Environ. Res. 172, 552–560.

Ma, J., Guo, H., Weng, L., Li, Y., Lei, M., Chen, Y., 2018a. Distinct effect of humic acid on ferrihydrite colloid-facilitated transport of arsenic in saturated media at different pH. Chemosphere 212, 794–801.

Ma, J., Guo, H.M., Lei, M., Li, Y.T., Weng, L.P., Chen, Y.L., et al., 2018b. Enhanced transport of ferrihydrite colloid by chain-shaped humic acid colloid in saturated porous media. Sci. Total Environ. 621, 1581–1590.

Mamindy-Pajany, Y., Hurel, C., Marmier, N., Roméo, M., 2011. Arsenic (V) adsorption from aqueous solution onto goethite, hematite, magnetite and zero-valent iron: effects of pH, concentration and reversibility. Desalination 281, 93–99.

Meng, J., Feng, X.L., Dai, Z.M., Liu, X.M., Wu, J.J., Xu, J.M., 2014. Adsorption characteristics of Cu(II) from aqueous solution onto biochar derived from swine manure. Environ. Sci. Pollut. Res. 21, 7035–7046.

Novikov, A.P., Kalmykov, S.N., Utsunomiya, S., Ewing, R.C., Horreard, F., Merkulov, A., et al., 2006. Colloid transport of plutonium in the far-field of the Mayak Production Association, Russia. Science 314, 638–641.

Phenrat, T., Saleh, N., Sirk, K., Kim, H.J., Tilton, R.D., Lowry, G.V., 2008. Stabilization of aqueous nanoscale zerovalent iron dispersions by anionic polyelectrolytes: adsorbed anionic polyelectrolyte layer properties and their effect on aggregation and sedimentation. J. Nanopart. Res. 10, 795–814.

Philippe, A., Schaumann, G.E., 2014. Interactions of dissolved organic matter with natural and engineered inorganic colloids: a review. Environmental Science & Technology 48, 8946–8962.

Ren, X.H., Sun, H.W., Wang, F., Zhang, P., Zhu, H.K., 2018. Effect of aging in field soil on biochar's properties and its sorption capacity. Environ. Pollut. 242, 1880–1886.

Shaaban, M., Van Zwieten, L., Bashir, S., Younas, A., Núñez-Delgado, A., Chhajro, M.A., et al., 2018. A concise review of biochar application to agricultural soils to improve soil conditions and fight pollution. J. Environ. Manag. 228, 429–440.

Shen, C.Y., Li, B.G., Chao, W., Huang, Y.F., Yan, J., 2011. Surface roughness effect on deposition of nano- and micro-sized colloids in saturated columns at different solution ionic strengths. Vadose Zone J. 10, 1071–1081.

Shen, C.Y., Wang, F., Li, B.G., Jin, Y., Wang, L.P., Huang, Y.F., 2012. Application of DLVO energy map to evaluate interactions between spherical colloids and rough surfaces. Langmuir 28, 14681–14692.

Shi, L., Yu, S., Wang, F.C., Wang, J., 2012. Pyrolytic characteristics of rice straw and its constituents catalyzed by internal alkali and alkali earth metals. Fuel 96, 586–594.

Song, W.P., Guo, M.X., 2012. Quality variations of poultry litter biochar generated at different pyrolysis temperatures. Journal of Analytical & Applied Pyrolysis 94, 138–145.

Tiberg, C., Gustafsson, J.P., 2016. Phosphate effects on cadmium(II) sorption to ferrihydrite. J. Colloid Interface Sci. 471, 103–111.

Torkzaban, S., Bradford, S.A., 2016. Critical role of surface roughness on colloid retention and release in porous media. Water Res. 88, 274–284.

Torkzaban, S., Tazehkand, S.S., Walker, S.L., Bradford, S.A., 2008. Transport and fate of bacteria in porous media: coupled effects of chemical conditions and pore space geometry. Water Resour. Res. 44, 159–172.

Tosco, T., Bosch, J., Meckenstock, R.U., Sethi, R., 2012. Transport of ferrihydrite nanoparticles in saturated porous media: role of ionic strength and flow rate. Environmental Science & Technology 46, 4008–4015.

Verwey, E.J.W., Overbeek, J.T.G., 1947. Theory of the stability of lyophobic colloids. Journal of Physical & Colloid Chemistry 51, 631–636.

Wang, D., Bradford, S.A., Harvey, R.W., Gao, B., Cang, L., Zhou, D., 2012. Humic acid facilitates the transport of ARS-labeled hydroxyapatite nanoparticles in iron oxyhydroxide-coated sand. Environmental Science & Technology 46, 2738–2745.

Wang, D., Zhang, W., Zhou, D., 2013. Antagonistic effects of humic acid and iron oxyhydroxide grain-coating on biochar nanoparticle transport in saturated sand. Environmental Science & Technology 47, 5154–5161.

Wang, D.J., Jin, Y., Jaisi, D.P., 2015. Effect of size-selective retention on the cotransport of hydroxyapatite and goethite nanoparticles in saturated porous media. Environmental Science & Technology 49, 8461–8470.

Wang, R.Z., Huang, D.L., Zhang, C., Liu, Y.G., Zeng, G.M., Lai, C., et al., 2019. Insights into the effect of chemical treatment on the physicochemical characteristics and adsorption behavior of pig manure-derived biochars. Environ. Sci. Pollut. Res. 26, 1962–1972.

Wei, Z.M., Zhao, X.Y., Zhu, C.W., Xi, B.D., Zhao, Y., Yu, X., 2014. Assessment of humification degree of dissolved organic matter from different composts using fluorescence spectroscopy technology. Chemosphere 95, 261–267.

Weng, L.P., van Riemsdijk, W.H., Koopal, L.K., Hiemstra, T., 2006. Adsorption of humic substances on goethite: comparison between humic acids and fulvic acids. Environmental Science & Technology 40, 7494–7500.

Woolf, D., Amonette, J.E., Street-Perrott, F.A., Lehmann, J., Joseph, S., 2010. Sustainable biochar to mitigate global climate change. Nat. Commun. 1, 56.

Xu, H., Ji, L., Kong, M., Jiang, H., Chen, J., 2019. Molecular weight-dependent adsorption fractionation of natural organic matter on ferrihydrite colloids in aquatic environment. Chem. Eng. J. 363, 356–364.

Yu, B., Jia, S.Y., Liu, Y., Wu, S.H., Han, X., 2013. Mobilization and re-adsorption of arsenate on ferrihydrite and hematite in the presence of oxalate. J. Hazard. Mater. 262, 701–708.